Activation cross section and isomeric cross-section ratio for the $(n, 2n)$ reaction on ^{191}Ir

N. Patronis,* C. T. Papadopoulos, S. Galanopoulos, M. Kokkoris, G. Perdikakis, and R. Vlastou
Department of Physics, National Technical University of Athens, Athens, Greece

A. Lagoyannis and S. Harissopulos
Institute of Nuclear Physics, NCSR "Demokritos," Athens, Greece
(Received 23 August 2006; published 16 March 2007)

The ^{191}Ir$(n, 2n)^{190}$Ir cross section was measured by means of the activation technique at four neutron energies in the range 10.0–11.3 MeV. The quasimonoenergetic neutron beam was produced via the ^{2}H$(d, n)^{3}$He reaction at the 5.5 MV Tandem Van de Graaff accelerator of NCSR "Demokritos." The cross section for the population of the second high spin (11^{-}) isomeric state was measured along with the sum of the reaction cross section populating both the ground (4^{-}) and the first isomeric state (1^{-}). Statistical model calculations taking into account pre-equilibrium emission were performed and compared with all the available experimental data. The experimentally deduced excitation function for populating both the ground and first isomeric state was well reproduced by the theoretical calculations. The statistical model calculations of populating the second metastable state revealed its strong dependence on the details of the introduced level scheme, as well as on the ratio between the effective moment of inertia and the rigid body moment of inertia of the residual nucleus. The experimental cross-section data corresponding to the second isomeric state and to the isomeric ratio were reproduced in a quite consistent way by the calculations.

DOI: 10.1103/PhysRevC.75.034607 PACS number(s): 24.10.−i, 24.60.Dr, 27.80.+w, 28.20.−v

I. INTRODUCTION

The study of neutron threshold reactions, and wherever it is possible of their isomeric cross-section ratio, is of considerable importance for testing nuclear models. In general, cross sections for the formation of isomeric states are more difficult to be predicted than those for the total reaction channels, since more details on the structure of the residual nucleus have to be taken into account (cf. Ref. [1]). The relative probability of forming isomeric states in a nucleus is mainly governed by the spin state values of the levels involved, and the spin distribution of the excited states of the compound nucleus. The high spin value 11^{-} of the second isomeric state (m2) of ^{190}Ir (Fig. 1) relative to the corresponding value 4^{-} of the ground state (g), offers great sensitivity for the study of the spin distribution of the residual nucleus.

The ^{191}Ir$(n, 2n)$ reaction and the isomeric cross section ratio $\sigma_{\mathrm{m2}}/\sigma_{\mathrm{g+m1}}$, have been studied in the past but only for incident neutron energies higher than 12 MeV (Refs. [2–12]). In these studies limited information concerning the level scheme of the odd-odd ^{190}Ir [13,14] was available. However, the details of the level scheme of the residual nuclei are very important to the isomeric cross-section ratio calculation, especially in the ^{191}Ir$(n, 2n)$ reaction, due to the high spin difference between the 11^{-} isomeric state (m2) and the ground state 4^{-}.

The purpose of this work was to experimentally deduce the ^{191}Ir$(n, 2n)^{190}$Ir$^{\mathrm{g+m1}}$ and ^{191}Ir$(n, 2n)^{190}$Ir^{m2} reaction cross section at the neutron beam energy range 10–12 MeV. Also, theoretical statistical model calculations were compared to all the available experimental data in an attempt to investigate spin dependence of the level density as well as the effective moment of inertia of the residual nucleus and their role in the formation of the isomeric state.

II. EXPERIMENTAL

A. Irradiations

The ^{191}Ir$(n, 2n)^{190}$Ir reaction cross section has been measured in the energy range between 10.0 and 11.3 MeV, by means of the activation technique. The neutron fluence for the cross section measurement was determined by using the monitor reaction ^{27}Al$(n, \alpha)^{24}$Na as Ref. [15]. In total, four irradiations were carried out at the 5.5 MV Tandem Van de Graaff accelerator of NCSR "Demokritos." Each irradiation lasted for ∼9 h, corresponding to ∼87% of the saturated activity of the second isomeric state $(11^{-})^{190}$Ir^{m2} (Fig. 1). The cross section for the formation of this state is lower than that for the population of the ground and first isomeric states ^{190}Ir^{g+m1}.

Two natural high-purity iridium foils (37.3% ^{191}Ir and 62.7%^{193}Ir) having a diameter of 13 mm were used for the irradiations. Each 0.5-mm-thick sample was sandwiched between identically shaped 0.5-mm-thick Al foils. This sample setup was sandwiched once more, between two gold foils, 0.25 mm in thickness and of equal diameter. Although the neutron flux was deduced from the Al foils, for which the ^{27}Al$(n, \alpha)^{24}$Na reaction cross section is well known, the activity of the Au foils was also measured aiming at the determination of the effect of parasitic neutrons to the cross section measurement, as described in Sec. II C.

The neutron beam was produced via the ^{2}H$(d, n)^{3}$He reaction, i.e., by bombarding the D_2 gas target [16] with deuteron beam currents, typically kept between 2 and 6 μA.

*Electronic address: patronis@central.ntua.gr

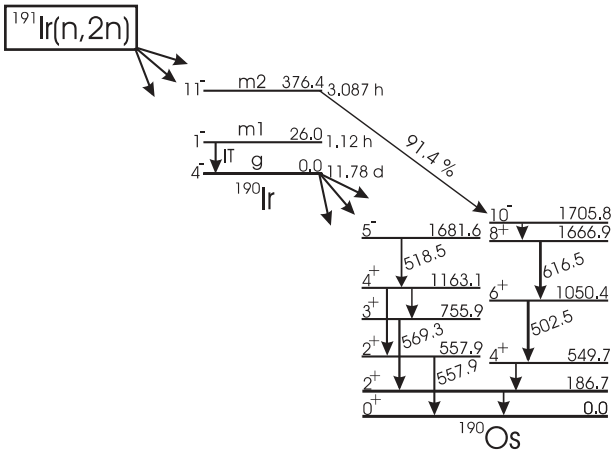

FIG. 1. Simplified representation of formation and decay of the ground state and isomeric states of ^{190}Ir [17]. All energies are in keV.

A 5-μm molybdenum foil served as the entrance window and a Pt foil as the beam stop of the gas cell. During the irradiations the gas target was cooled through a cold air jet to minimize the effect of heating in the deuterium gas pressure, which was continuously controlled through a micrometric valve. Using this setup, a flux of the order of $\sim 4 \times 10^6$ n/(cm^2·s) was achieved.

The neutron flux was monitored by a BF_3 counter placed at 0° with respect to the neutron beam and at a distance of 3 m from the deuteron gas target. The neutron yield, as measured by the BF_3 detector, was recorded at regular time intervals (40 s) by means of a multichannel scaler. This neutron flux history file was used in the analysis, for off-line correction of the fraction of ^{190}Ir nuclei, which had already decayed during activation. The sample sandwich was placed at 0° with respect to the neutron beam and at a distance of 7 cm from the center of the gas cell. At this distance, the angular acceptance of the samples setup was less than ±5.5°. During the irradiations, the gas cell was constantly operated at a pressure of 1100 mbar, to keep the uncertainty of the neutron beam energy distribution, as low as possible.

The main quantities concerning the irradiations of the samples are summarized in Table I.

B. Activity measurements

Following the irradiations, the induced activity on the samples was measured with a 56% relative efficiency HPGe detector. The source to detector distance was more than 10 cm. At this distance any corrections for pile up or coincidence summing effects were negligibly small.

The population of the second isomeric state (m2) was measured independently through the 502- and 616-keV lines (Fig. 1), where the contribution from the decay of the ground state was small, i.e., ∼8% for the 502.5-keV transition and ∼3% for the 616.5-keV transition. The intensity measurement of these lines, originating from the decay of the 11$^-$ isomeric state, started 2–4 h after the end of the irradiation and lasted for ∼10 h. The induced activity on the aluminum foils was determined afterwards using the same experimental setup.

TABLE I. Summary of the irradiation parameters.

	10.0 MeV	10.5 MeV	11.0 MeV	11.3 MeV
Irradiation time (h)	7.07	10.13	9.45	9.02
Integrated flux ($\times 10^{11}$) (cm^{-2})	1.02±0.05	1.07±0.06	1.35±0.07	1.36±0.07
Measuring time[a] (h)	19.27/10.0	42.4/10.0	15.46/11.0	16.77/11.0
Decay correction f_B[a]	0.991/0.501	0.988/0.393	0.989/0.416	0.989/0.438

[a]For these parameters two values are given: A/B. A corresponds to the measurement σ_{g+m1} and B to the σ_{m2} one.

In less than 1 h the activity of the aluminum foils could be determined with a statistical error better than 2%. The sum of the cross sections for the population of the first isomeric state (m1) and the ground state (g), was determined via the 518.5-, 557.9-, and 569.3-keV transitions (Fig. 1). These transitions were free from any contribution coming from the decay of the second isomeric state. The measurement of the activity related to the decay of the ground state, started ∼16 h after the end of the irradiation. In this way, it was ensured that the 1$^-$ isomeric state (m1) with a half-life $T_{1/2} = 1.12h$, has fully decayed to the ground state. This procedure was necessary to correctly evaluate the sum of the ^{190}Ir^{m1} and ^{190}Ir^{g} population, because the decay of the first metastable state (m1) is not accompanied by γ emission. The contribution of the decay of the second isomeric state (m2) to the σ_{g+m1} cross section was calculated taking into account the relevant cross sections and branching ratios of the updated level scheme [17] and was found to be less than 0.4% in all cases. Figure 2 shows the γ-ray spectra emitted by the iridium sample during the 42-h measurement of the decay of the ground state (lower spectrum) and the 10-h measurement of the decay of the ^{190}Ir^{m2} isomeric

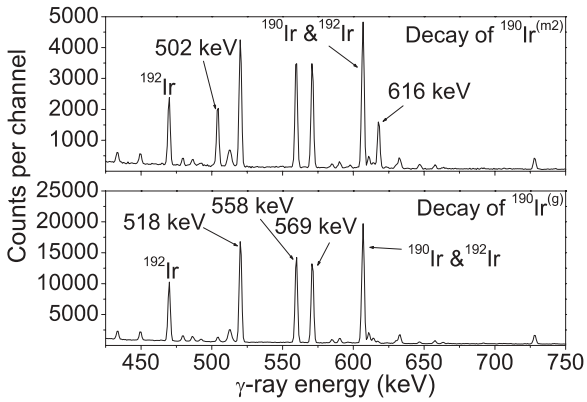

FIG. 2. Part of the γ-ray spectra of the 10.5-MeV run. The upper spectrum corresponds to decay measurement of the second isomeric state 11$^-$ and the lower spectrum to the decay measurement of the ground state of ^{190}Ir. In the analysis only the lines indicated with their energy values were used.

state (upper spectrum). In both spectra the prominent line at 605 keV can also be observed. However, this transition could not be used in the analysis, due to its contamination from the 604 keV transition from the decay of the ^{192}Ir isotope, which was produced during the irradiation, via the ^{193}Ir$(n, 2n)^{192}$Ir reaction.

C. Neutron spectra

The neutron energy distribution in the samples was deduced according to the analytical approach described by Klein *et al.* [18], taking into account the energy loss and straggling of the deuteron beam at the entrance foil and at the deuterium gas. Also, the sample geometry and distance from the gas cell were adjusted so that the width of the neutron beam energy distribution that the sample subtends be less than 0.1 MeV.

The contribution of background "parasitic" neutrons, originating from the interaction of the deuteron beam with the gas cell structural materials, has been verified experimentally via sequential gas-in and gas-out measurements [19], implementing the multiple foil activation technique. This contribution of the "parasitic" neutrons, bearing energies high enough to activate the ^{27}Al reference foil, did not exceed 3% in the least favourable case ($E_n = 11.3$ MeV). Despite the lower threshold of the ^{27}Al(n, α) reference reaction, compared to the $(n, 2n)$ reactions on ^{197}Au and ^{191}Ir, the values of the neutron flux as deduced from the Au and Al foils were in excellent agreement. This verifies the fact that the contribution of "parasitic" neutrons originating both from deuteron break up and the interaction of the beam with the structural materials of the gas cell, is negligible for high threshold reactions such as the ones considered in the present work. Since the ^{197}Au$(n, 2n)$ reaction threshold ($E_{\text{thr}} = 8.1$ MeV) and the shape of its excitation function are similar to that of the ^{191}Ir$(n, 2n)$ reaction, the contribution of the small "parasitic" part of the flux to the activation of Al and Ir foils is expected to compensate each other at the final calculation of the $(n, 2n)$ reaction cross section. Thus, no correction was necessary to account for the presence of those "parasitic" neutrons.

III. DATA ANALYSIS

For each run, the neutron flux irradiating the iridium sample was measured via the ^{24}Na activity induced at the front and back aluminum foils. The total number of activated nuclei at the end of the irradiation

$$A = \frac{\Delta N C_A C_{DT}}{(1 - e^{-\lambda t_m}) e^{-\lambda t_w} \epsilon I} \tag{1}$$

could be derived from the number of counts ΔN in the 1369-keV line of ^{24}Na. The factors C_A, C_{DT} correspond to self-attenuation and dead-time corrections, respectively. The measuring time and the time interval between the end of the irradiation and the beginning of the measurement are denoted as t_m and t_w, respectively. The factors λ, ϵ, and I are the decay rate of ^{24}Na, the absolute efficiency of the HPGe detector, and the intensity of the 1369-keV line, respectively.

TABLE II. Decay properties of the product nuclei.

Product nucleus	Half-life	γ-ray energy (keV)	Intensity per decay (%)
^{190}Ir^{g} [a]	11.78 ± 0.10 d	518.5	34.0 ± 1.5
		558.0	30.1 ± 1.3
		569.3	28.5 ± 1.3
^{190}Ir^{m2} [a]	3.087 ± 0.012 h	502.5	89.4 ± 0.2
		616.5	90.1 ± 0.2
^{24}Na [b]	14.9590 ± 0.0012 h	1368.6	100 ± 0.0

[a]Reference [17].
[b]Reference [20].

The γ-ray intensities and half-lives used in the analysis are summarized in Table II. The time integrated neutron flux Φ_{tot} for each aluminum foil was deduced after combining Eq. (1) with the well-known activation equation

$$A = \Phi_{\text{tot}} N \sigma f_B, \tag{2}$$

where the factor N corresponds to the number of sample atoms per cm^2, whereas σ is the cross section of the ^{27}Al$(n, \alpha)^{24}$Na reaction as obtained from the IRDF-2002 database [15]. The time factor f_B corrects for the decay during activation, including the effects due to time variations of the neutron flux [21]. By averaging over the induced activities of the front and back aluminum foils, one is able to correct for target geometry, neutron scattering, and self-shielding.

The measured activity from the decay of the second isomeric state (^{190}Ir^{m2}) was corrected for the contribution from the decay of the ground state. Furthermore, the appropriate corrections were applied for the self-attenuation of γ rays in the iridium sample and for the extended geometry of the samples. This correction factor was determined by means of GEANT4 [22] Monte Carlo calculations, where the full experimental setup was included.

By combining Eqs. (1) and (2), and using the average neutron flux through the aluminum foils, the sample cross section could be deduced.

The corresponding uncertainties were obtained by summing up quadratically all the possible individual errors that are summarized in Table III. The uncertainties in the time factors and the counting statistics were negligible. It should also be

TABLE III. Compilation of uncertainties.

	Uncertainty %
^{27}Al$(n, \alpha)^{24}$Na cross section	2
Detector efficiency	4
Correction factors	2
Measurement of neutron flux	5.2
Counting statistics [a]	0.5–0.9/1.1–2.0
Time factors	<0.5
γ-ray intensity per decay [a]	4.5/0.2
Total uncertainty of cross section	6.1–6.4

[a]For these factors two values of uncertainty are given: A/B. A corresponds to the uncertainty of σ_{g+m1} measurement and B to σ_{m2}.

noticed (Table II) that high uncertainties are introduced to the cross-section calculation by the relative γ-ray intensities from the decay of the ground state of ^{190}Ir.

IV. THEORETICAL CALCULATIONS

In the region of 5–25 MeV the dominant reaction mechanism of neutron interaction is the compound and precompound nucleus processes. Cross sections calculations were performed in the framework of the Hauser-Feshbach theory [23] for the equilibrium process, whereas the pre-equilibrium effects were taken into account via the exciton model [24]. The STAPRE-F [25] code, which was applied, is designed to estimate energy-averaged cross section for the particle-induced reactions with several emitted particles (n, p, d, α) and γ rays, under the assumption of sequential evaporation. In this work, the contribution to the denominator of the Hauser-Feshbach equation, corresponding to the charged-particles emission was ignored, because in the heavy mass region $A \geqslant 190$, neutron reactions with charged-particle emission are strongly hindered by the Coulomb barrier. Each evaporation step is treated in the framework of the statistical model, taking into consideration the angular momentum and parity conservation, as well as the pre-equilibrium decay in the first particle emission.

The exciton model assumes that after the initial interaction between the incident particle and the target nucleus, the excited system can pass through a series of stages of increasing complexity before equilibrium is reached. Neutron emission may occur from these states yielding the pre-equilibrium neutrons. Pre-equilibrium emission of the first neutron causes a reduction of the population that reaches the equilibrium stage, i.e., of the cross section for the formation of the equilibrate compound nucleus. The pre-equilibrium emission factor is determined by the square matrix element $|M|^2 = KA^{-3}E_n^{-1}$, where A is the mass number of the nucleus, E_n is the incident neutron energy, and K is the free parameter of the model. This parameter can be estimated experimentally by the hard component of the spectrum of inelastically scattered neutrons or from the shape of the excitation function of $(n, 2n)$ or $(n, 3n)$ reactions. In the present work, the best value for the K parameter as obtained from the available experimental data was equal to 200.

The excited state of the compound nucleus de-excites either by neutron emission to another isotope or by γ-ray cascade to the ground state or to the isomeric state of the residual nuclei. The γ-ray transmission coefficients are also of considerable significance. The strength functions for multipole radiation $M1$, $E2$, $M2$, and $E3$ were calculated according to the Weisskopf model, based on the single particle estimation and normalized to the $E1$ strength function, which was obtained by means of the Brink-Axel hypothesis [26,27]. The $E1$ strength function was normalized to reproduce the experimentally observed average total radiation width $\langle \Gamma_\gamma \rangle$ at the neutron binding energy, as it was provided by Ignatyuk [28].

In the continuum region, the level density was calculated using the generalized superfluid model (GSM), in the form of the phenomenological model provided by Ignatyuk *et al.* [29], which takes into account, shell, pairing. and collective effects in a consistent way.

The dependence of the level density $\varrho(U, J)$ on the excitation energy U can be separated from the function of spin distribution $f(J)$ in a proportional form

$$\varrho(U, J) \propto \rho(U) f(J), \tag{3}$$

where

$$f(J) = R(2J+1)e^{-J(J+1)/2\sigma_{\text{eff}}^2} \tag{4}$$

The parameter R represents the dependence of $f(J)$ on the shape and symmetry of the nucleus and σ_{eff}^2 is the spin cut-off parameter.

At the GSM, the level density needs to be treated separately in two energy regions depending on the nucleus temperature t. The normal phase $t \geqslant t_{\text{cr}}$ or $U' \geqslant U_{\text{cr}}$ and the superfluid phase $t < t_{\text{cr}}$ or $U' < U_{\text{cr}}$, where the level density expressions have to change according to the simple parametrization proposed in Ref. [29]. The level density is expressed in terms of the effective excitation energy $U' = U + n\Delta_0$, where U is the true excitation energy of the compound nucleus and $n = 0, 1, 2$ for even-even, even-odd, and odd-odd nucleus, whereas $\Delta_0 = 12/\sqrt{A}$ is the pairing correlation function that is related to the critical temperature $t_{\text{cr}} = 0.567\Delta_0$. The level density parameter α is calculated according to the following equation

$$\alpha = \begin{cases} \tilde{a}\left[1 + \frac{\delta\epsilon_0}{U' - E_{\text{cond}}} f(U' - E_{\text{cond}})\right], & U' \geqslant U_{\text{cr}} \\ \alpha_{\text{cr}}, & U' < U_{\text{cr}}, \end{cases} \tag{5}$$

where $\tilde{a}$ is the asymptotic value of α at high excitation energy, $\delta\epsilon_0$ is the shell correction of the nuclear binding energy, calculated from the difference between the experimental mass of nucleus and the liquid drop model mass. The dimensionless function $f(U')$ determines the energy behavior of α [30]. The critical energy is given by $U'_{\text{cr}} = \alpha_{\text{cr}} t_{\text{cr}}^2 + E_{\text{cond}}$, where $E_{\text{cond}} = (3/2\pi^2)\alpha_{\text{cr}}\Delta_0^2$ characterizes the decrease of the ground-state energy of the superfluid phase relative to the Fermi-gas phase.

For axially symmetric nuclei the value of the spin cut-off parameter is related to the perpendicular axis moment of inertia and the temperature of the compound nucleus

$$\sigma_{\text{eff}}^2 = \Theta_\perp t/\hbar^2, \tag{6}$$

where

$$\Theta_\perp = \begin{cases} \Theta_{\text{rig}}\left(1 + \frac{1}{3}\varepsilon\right), & U' \geqslant U_{\text{cr}} \\ \Theta_\perp^\circ + \left(\Theta_\perp^{\text{cr}} - \Theta_\perp^\circ\right)\frac{t_c}{t}(1 - \varphi^2), & U' < U_{\text{cr}} \end{cases} \tag{7}$$

ε is the quadrupole deformation parameter, $\Theta_\perp^\circ$ is the perpedicular moment of inertia in the ground state, and the function φ is given by the expression

$$\varphi = (1 - U'/U_{\text{cr}})^{1/2}. \tag{8}$$

The GSM parameters used in the calculations were taken from the literature and are summarized in Table IV. For $\Theta_\perp^\circ$ several values have been used in the region 20–30$\hbar^2$ MeV^{-1}, as derived from the empirical estimate $\Theta_{\text{rig}}/3$ in consistency with the experimentally deduced rotational band of the neighboring nucleus ^{190}Os, without altering the results.

The transmission coefficients for neutrons that determine the absorption probability as well as the particle emission

TABLE IV. Statistical model calculation parameters.

Parameter	^{192}Ir	^{191}Ir	^{190}Ir	^{189}Ir	Reference
$\tilde{a}$, asymptotic value of main level density parameter (MeV^{-1})	16.4	16.3	16.2	16.1	[28]
$n\Delta_0$, odd even excitation energy shift (MeV)	1.74	0.87	1.74	0.87	[25]
$\delta\epsilon_0$, shell correction (MeV)	−1.621	−1.321	−0.913	−0.718	[28,31]
ϵ, quadrupole deformation parameter	0.145	0.155	0.164	0.164	[32]
Neutron separation energy (MeV)	6.20	8.03	6.37	8.20	[33]
Average experimental total radiation width (meV)	100	81	90[a]	80[a]	[28]

[a]These values were not included in the average parameters of s- and p-wave neutron resonances provided by A. V. Ignatyuk and were deduced according to the neighboring nuclei values.

probability were calculated by the code ECIS03 [34], using the global parameters of Koning and Delaroche [35].

The energies, spin, parities, and branching ratios of the discrete levels for the iridium isotopes were selected from Nuclear Data Sheets [17,36,37]. For the calculation of the isomeric cross section ratio, the first 48 discrete levels of ^{190}Ir were used.

V. RESULTS AND DISCUSSION

The experimental results of this work for the ^{191}Ir$(n, 2n)^{190}$Ir^{g+m1} and ^{191}Ir$(n, 2n)^{190}$Ir^{m2} reactions, as well as the isomeric ratio values are presented in Table V along with their uncertainties. All the data reported in this work in the energy range 10.0–11.3 MeV have been determined for the first time. This is a critical energy region, just above the threshold of the reaction, where the cross section varies rapidly until it reaches the plateau around 14 MeV, where many data exist in literature with large discrepancies among them. The only existing data at lower incident neutron energies are at 8.6 and 9.3 MeV [38], where only the sum of the cross section was measured for the population of the ground state (g) and the first isomeric state (m1). In addition, for the ^{191}Ir$(n, 2n)^{190}$Ir reaction, the partial cross section for one γ transition ($E_\gamma = 117.3$ keV, $6^+ \rightarrow 5^+$), was reported in the past by Fotiades *et al.* [39].

A. Cross sections and excitation functions

The experimental cross section data for populating the ground and first isomeric state of ^{190}Ir are shown in Fig. 3 along with all the previous measurements reported in the literature. The data provided in this work are in excellent agreement, with the trend of the existing experimental data.

TABLE V. Cross sections for the ^{191}Ir$(n, 2n)^{190}$Ir^{g+m1} and ^{191}Ir$(n, 2n)^{190}$Ir^{m2} reactions.

Energy (MeV)	σ_{g+m1} (mb)	σ_{m2} (mb)	$\sigma_{m2}/\sigma_{g+m1}$
10.0	1090 ± 70	25.7 ± 1.6	0.024 ± 0.001
10.5	1400 ± 90	44.4 ± 2.8	0.032 ± 0.002
11.0	1550 ± 100	60.0 ± 3.7	0.039 ± 0.002
11.3	1640 ± 100	65.4 ± 4.0	0.040 ± 0.002

The cross section σ_{m2} of populating the high-spin second isomeric state was measured independently and the corresponding data are presented in Fig. 4. The existing experimental cross section data for populating this 11^- state (also included in Fig. 4) are rather discrepant, particularly in the high neutron beam energy region, where more than one data set is available. However, our data are in agreement with the general trend of all the data sets.

The theoretical calculations obtained by using the parameters described in the previous section are presented with the dotted line, in Figs. 3 and 4. The experimental σ_{g+m1} values are fairly well reproduced by this calculation (dotted line), whereas for the σ_{m2}, the theoretical predictions for populating the 11^- isomer overestimate the experimental data in the high-energy region, despite the large discrepancies.

The attempt to better reproduce the data by varying within reasonable limits the parameters affecting the energy dependence of the nuclear level density ($\tilde{a}$, ε, etc.), as well as the total radiation width affecting the γ ray strength, provided no significant change of the theoretical calculations. Similar results were obtained, for different assumptions concerning the shape and symmetry (axially symmetric, triaxial, etc.) of the Ir isotopes, that belong to the transitional region from well deformed to spherical nuclei [40].

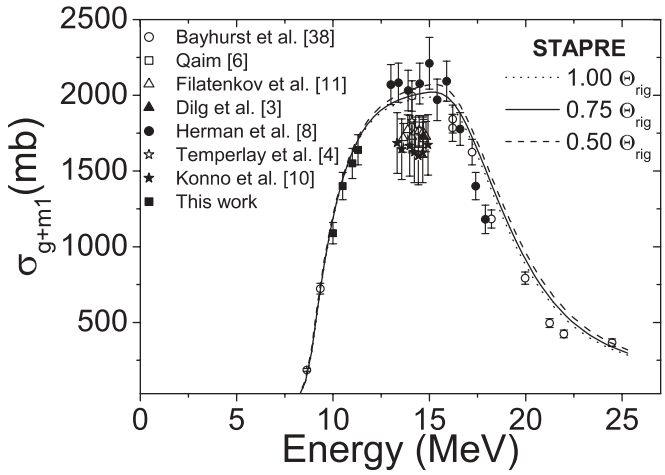

FIG. 3. The measured and calculated cross section σ_{g+m1} for the population of the ground and first isomeric state of ^{190}Ir.

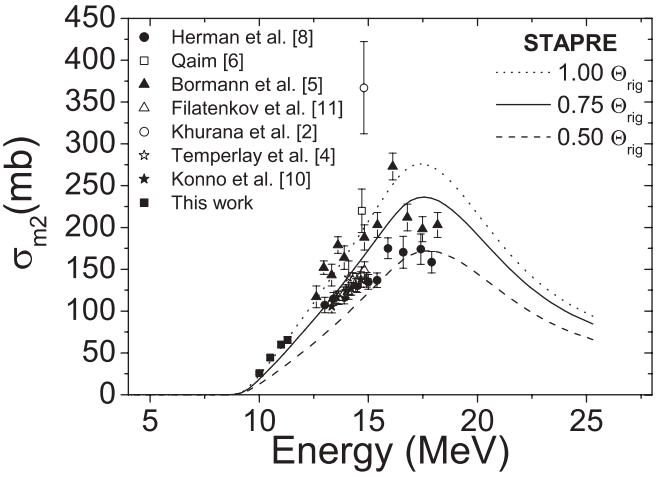

FIG. 4. The measured and calculated cross section σ_{m2} for the population of the second isomeric state of ^{190}Ir.

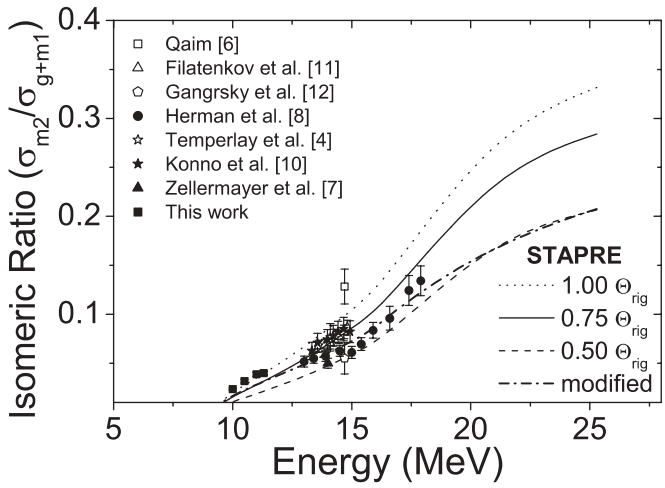

FIG. 5. The isomeric cross section ratio $\sigma_{m2}/\sigma_{g+m1}$, calculation and experimental results.

This behavior of the calculations for the σ_{m2} and σ_{g+m1} cross sections, is attributed to the fact, that only a small part of the continuum de-excites by feeding high spin states of the discrete. This part of the continuum, is strongly dependent on the spin cut-off parameter σ^2 and consequently, on the perpendicular moment of inertia, $\Theta_\perp$ and Θ_{rig} [Eqs. (6) and (7)]. This fact results to a reduction of the population rates of higher spin levels, compared to their low-spin counterparts, which becomes more pronounced as the populated level spin is increased.

To further study this dependence on the moment of inertia, theoretical calculations using Θ_{rig} values lowered by 25 and 50% (keeping the perpendicular moment of inertia of the ground state $\Theta^0_\perp$ and the quadrupole deformation parameter ε, fixed), were carried out, and are presented in Figs. 3 and 4 by the solid and the dashed line, respectively. The results of the calculations show that the population of high- and low-spin states is strongly dominated by the spin distribution of the level density. The lowering of Θ_{rig} causes a significant decrease of the high-spin level cross section σ_{m2} (Fig. 4), whereas the low-spin cross section σ_{g+m1}, gets equally increased. However, this increase is very small compared to the cross section for populating the (g) and (m1) levels σ_{g+m1}. Thus the calculation for the σ_{g+m1} cross section remains in agreement within the errors of the experimental points throughout the energy range (Fig. 3).

To better reproduce the experimental data for the high-spin isomer, it seems that the rigid body moment of inertia Θ_{rig}, should be decreased by a factor of the order of 25%. This is surprising result according to the superfluid model of the nucleus, because for excitation energies above the critical point of phase transition, the pairing interaction should disappear. Similar results have been previously reported from theoretical calculations and from the interpretation of experimental data [41,42].

B. Isomeric cross-section ratio

The isomeric cross-section ratio of $\sigma_{m2}/\sigma_{g+m1}$ deduced from the experimental cross-section data, is presented in Fig. 5. The ratio is low in the low-energy region and rises at higher beam energies, following the rise in the population of high spin levels of the compound nucleus, by the increase of the incident particle energy.

The theoretical ratio resulting from the calculations of σ_{m2} and σ_{g+m1} (dotted line in Fig. 5) is retaining the trend of overestimating the data that are exaggerated in the high-energy region, whereas for low energies there is a fair agreement between the data and the calculated isomeric cross-section ratio.

The reduced values of Θ_{rig}, tried in the calculations, produced lower predictions, an effect similar to that for the isomeric cross section σ_{m2}, which is expected, because only the numerator of the isomeric cross-section ratio changes significantly by varying the parameter Θ_{rig}.

Indeed, the experimental data of the low-energy region are reproduced fairly well without altering the Θ_{rig} value (dotted line), whereas at higher energy regions, the experimental data can be approached only by reducing the value of Θ_{rig} by 25–50% (solid and dashed lines in Fig. 5, respectively).

However, a reduction of the order of 25% on the value of Θ_{rig} (solid line Fig. 5) is sufficient for an acceptable reproduction of all the available data, throughout the energy region considered in this work.

A more detailed consideration of the trend exhibited by the available experimental data reveals three different energy regions. (i) The low-energy region, which extends up to neutron beam energies of 11.7 MeV. This energy value corresponds for the ^{190}Ir nucleus to a true excitation energy of 3.7 MeV above the threshold of the ^{191}Ir$(n, 2n)$ reaction or, equivalently, to an effective excitation energy $U' = 5.44$ MeV. This excitation energy corresponds to the critical energy of phase transition, U_{cr}, in the calculation of the level density of the ^{190}Ir nucleus [Eqs. (5)–(8)]. (ii) The middle-energy region, between 11.7 and 14.5 MeV, and (iii) the high-energy region above 14.5 MeV, which is close to the neutron separation energy and permits the $(n, 3n)$ channel to open. The trend of the excitation function in these regions is generally increasing, apart from the middle-energy region, where a plateau is reached. This trend becomes clear by excluding the single data points around 14 MeV, corresponding to the experimental points in Fig. 3 that are lower than the general trend of the data.

This behavior of the slope discontinuities could be attributed to changes in the moment of inertia, which is a dynamical quantity depending on the excitation energy. In the GSM model, to account for shell pairing and collective effects, $\Theta_\perp$ is proposed to increase from $\Theta_\perp^0$ to $\Theta_\perp^{cr} = \Theta_\perp$ in the region up to U_{cr}, which separates the superfluid from the normal phase, and to remain constant to $\Theta_\perp = \Theta_{rig}(1 + \varepsilon/3)$ thereafter [Eq. (7)].

Even though the concept of a varying moment of inertia is incorporated in the model, the calculations failed to accurately reproduce the different slopes of the data. The only way to describe the behavior of the experimental data as shown by the dashed-dotted line in Fig. 5 (modified) would be to adopt a reduced by 50% value of Θ_{rig}, while at the same time, in contrast to Eq. (7), below the critical energy of phase transition U_{cr}, the moment of inertia should increase for decreasing values of excitation energy, until the value of $\Theta_\perp^0$ is reached, which in any case should be higher than the 50% reduced value of Θ_{rig}.

Such an anomalous behavior of the moment of inertia is surprisingly unexpected in the framework of the GSM model. However, recent microscopic calculations for the iron region revealed the possible presence of strong odd-even effects in the spin distribution of the level density in the form of a rise of the moment of inertia at low temperatures [43].

Another point should be made on the dependence of the calculations for the isomeric ratio on the level scheme of the residual nucleus. The isomeric cross-section ratio is governed by the details of the discrete level scheme introduced to the calculations. ^{190}Ir is an odd-odd nucleus in the transition region between spherical and deformed nuclei with a complex structure so that the detailed reproduction of the level scheme in the calculations is a difficult task. In particular, the appearance of the high-spin 11^- isomeric state among the low-lying excited states results from high-spin intruder configurations $\pi 11/2[552] \otimes \nu 11/2[615]$ and inhibits its communication with neighboring discrete levels. It should be underlined that the details of the level scheme became known only recently [17]. On previous Nuclear Data sheets for $A = 190$ [13,14], only the energy, spin, and parity of the ground, first, and second isomeric state were given. The spin and parity of the ground and first isomeric state were (4^+) and (7^+), respectively, instead of the latest reported values (4^-) and (1^-). The new spin and parity values of the most recent compilation [17] resulted after considering the work of Garrett *et al.* [40,44]. Apart from the corrected spin and parity values of the ground and first isomeric state, in the most recent compilation [17] the second isomeric state (11^-) was pushed up in energy from 175 to 376 keV. These updates concerning the discrete level scheme were taken into account in the calculations. For the rest of the level scheme, in cases where the spin and parity were not known, estimates from neighboring levels were adopted. The cumulative plot of the discrete levels taken from Ref. [17] was fitted by the GSM level density formula. These changes were found to be quite important to the theoretical calculation of the isomeric cross-section ratio, which has been performed for the first time in this work for a wide energy range.

It is interesting to note that Ir isotopes belong to the transition region from well-deformed to spherical nuclei and exhibit a very complex structure (γ-softening, triaxiality, shape coexistence) [40]. Despite the fact that in this region the level density calculations are supposed to be rather rough [29], in the present work the general trend of the experimental data is fairly reproduced. However the details of the excitation function of the high-spin isomeric cross section ratio has to be further studied theoretically and experimentally in the region $A = 190$.

VI. CONCLUSIONS

The cross section of the $(n, 2n)$ reaction on ^{191}Ir, was measured independently for the population of the second isomeric state (σ_{m2}), and for the sum of the reaction cross section for the population of the ground and the first isomeric state (σ_{g+m1}). The cross-section values were determined by means of the activation technique at the neutron beam energy range 10.0–11.3 MeV for the first time. Nuclear model calculations using the code STAPRE-F were performed taking into account the new up-to-date information on the level scheme of ^{190}Ir, which was crucial for the determination of the isomeric cross-section ratio.

The calculations proved that the GSM model is suitable for calculating effectively the nuclear level density even in the region of transitional nuclei that is characterized by complex nuclear structure properties.

The theoretical results for the cross section of the second isomeric state as well as for the isomeric cross-section ratio verified the strong dependence of the corresponding cross sections on the spin distribution of the level density and, more specifically, on the effective moment of inertia. It is of great interest that a significantly reduced value of the rigid body moment of inertia by at least a factor of 25% is required to obtain an acceptable description of the high-spin isomer population cross section, for energies well above the point of phase transition, where the pairing interaction should seize to affect the nuclear level density.

Finally, evidence for an energy dependence of the moment of inertia distinctly different to the one adopted in the framework of the superfluid model was presented, based both on the trend of the experimental data as well as on the results of theoretical calculations. However, further studies of this energy dependence have to be carried out both from the experimental and from the theoretical point of view in the region around $A = 190$, before a firm conclusion is drawn.

ACKNOWLEDGMENTS

We thank N. Divis, N. Papakostopoulos, and V. Andreopoulos for their support during the measurement at the Tandem Van de Graaff accelerator as well as A. Asthenopoulos for his excellent technical assistance. The project is cofunded by the European Social Fund (75%) and National Resources (25%)–(EPEAEK-II)–PYTHAGORAS II.

[1] S. M. Qaim, A. Mushtaq, and M. Uhl, Phys. Rev. C **38**, 645 (1988).
[2] C. S. Khurana and H. S. Hans, Nucl. Phys. **28**, 560 (1961).
[3] W. Dilg, H. Vonach, G. Winkler, and P. Hille, Nucl. Phys. **A118**, 9 (1968).
[4] J. K. Temperley and D. E. Barnes, Ballistic Research Labs Reports, No. 1491, (1970).
[5] M. Bormann, H. H. Bissem, E. Magiera, and R. Warnemünde, Nucl. Phys. **A157**, 481 (1970).
[6] M. Qaim, Nucl. Phys. **A185**, 614 (1972).
[7] D. M. Zellermayer and B. Rosner, Phys. Rev. C **6**, 315 (1972).
[8] M. Herman, A. Marcinkowski, and K. Stankiewicz, Nucl. Phys. **A430**, 69 (1984).
[9] A. Reggoug and M. Beradda, Nucl. Instrum. Methods Phys. Res. A **255**, 107 (1987).
[10] C. Konno, Y. Ikeda, K. Oishi, K. Kawade, H. Yamamoto, and H. Maekawa, JAERI Tokai report series, No. 1329 (1993).
[11] A. A. Filatenkov and S. V. Chuvaev, Khlopin Radiev. Inst., Leningrad Reports No. 259 (2003).
[12] Yu. P. Gangrsky, N. N. Kolesnikov, V. G. Lukashik, and L. M. Melnikova, Phys. At. Nucl. **67**, 1227 (2004).
[13] C. M. Lederer, Nucl. Data Sheets **35**, 525 (1982).
[14] B. Singh, Nucl. Data Sheets **61**, 243 (1990).
[15] The International Reactor Dosimetry File 2002, Nuclear Data Section, IAEA, Vienna.
[16] G. Vourvopoulos, T. Paradellis, and A. Asthenopoulos, Nucl. Instrum. Methods Phys. Res. **220**, 23 (1984).
[17] B. Singh, Nucl. Data Sheets **99**, 275 (2003).
[18] H. Klein, H. J. Brede, and B. R. L. Siebert, Nucl. Instrum. Methods Phys. Res. **193**, 635 (1982).
[19] G. Perdikakis, C. T. Papadopoulos, R. Vlastou, A. Lagoyannis, A. Spyrou, M. Kokkoris, S. Galanopoulos, N. Patronis, D. Karamanis, Ch. Zarkadas, G. Kalyva, and S. Kossionides, Phys. Rev. C **73**, 067601 (2006).
[20] R. B. Firestone, *Table of Isotopes*, 8th ed. (Wiley Interscience, New York, 1996).
[21] H. Beer and F. Käppeler, Phys. Rev. C **21**, 534 (1980).
[22] GEANT4-A simulation toolkit, S. Agostinelli *et al*., Nucl. Instrum. Methods. Phys. Res. A **506**, 250 (2003).
[23] W. Hauser and H. Feshbach, Phys. Rev. **87**, 366 (1952).
[24] J. J. Griffin, Phys. Rev. Lett. **17**, 478 (1966).
[25] M. Uhl and B. Strohmaier, IRK-76/01, IRK, Vienna (1976).
[26] D. M. Brink, Ph.D. thesis, Oxford University (1955).
[27] P. Axel, Phys. Rev. **126**, 671 (1962).
[28] T. Belgya, O. Bersillon, R. Capote, T. Fukahori, G. Zhigang, S. Goriely, M. Herman, A. V. Ignatyuk, S. Kailas, A. Koning, P. Oblozinsky, V. Plujko, and P. Young, Handbook for calculations of nuclear reaction data, RIPL-2, IAEA-TECDOC-1506 (IAEA, Vienna, 2006). Available online at http://www-nds.iaea.org/RIPL-2/
[29] A. V. Ignatyuk, K. K. Istekov, and G. N. Smirenkin, Sov. J. Nucl. Phys. **29**, 450 (1979).
[30] A. V. Ignatyuk, J. L. Weil, S. Raman, and S. Kahane, Phys. Rev. C **47**, 1504 (1993).
[31] W. D. Myers and W. J. Swiatecki, Ark. Fizik **36**, 343 (1967).
[32] P. Moller, J. R. Nix, W. D. Myers, and W. J. Swiatecki, At. Data Nucl. Data Tables **59**, 185 (1995).
[33] G. Audi, A. H. Wapstra, and C. Thibault, Nucl. Phys. **A729**, 337 (2003).
[34] J. Raynal, "Notes on ECIS 94," Note CEA-N-2772 (1994).
[35] A. J. Koning and J. P. Delaroche, Nucl. Phys. **A713**, 231 (2003).
[36] C. M. Baglin, Nucl. Data Sheets **84**, 717 (1998).
[37] E. Browne and S. Y. Chu, Nucl. Data Sheets **74**, 611 (1995).
[38] B. P. Bayhurst, J. S. Gilmore, R. J. Prestwood, J. B. Wilhelmy, Nelson Jarmie, B. H. Erkkila, and R. A. Hardekopf, Phys. Rev. C **12**, 451 (1975).
[39] N. Fotiades, R. O. Nelson, M. Devlin, M. B. Chadwick, P. Talou, J. A. Becker, P. E. Garrett, and W. Younes, Lawrence Livermore National Laboratory, UCRL-PROC-209031 (2005).
[40] P. E. Garrett, H. Baltzer, M. Bertschy, D. G. Burke, M. Délèze, S. Drissi, C. Günther, J. Jolie, J. Kern, H. Lehmann, S. J. Mannanal, J. Manns, U. Müller, J. P. Vorlet, N. Warr, and T. Weber, Nucl. Phys. **A662**, 235 (2000).
[41] S. F. Mughabghab and C. Dunford, Phys. Rev. Lett. **81**, 4083 (1998).
[42] M. Al-Abyad, S. Sudár, M. N. H. Comsan, and S. M. Qaim, Phys. Rev. C **73**, 064608 (2006).
[43] Y. Alhassid, G. F. Bertsch, L. Fang, and S. Liu, Phys. Rev. C **72**, 064326 (2005).
[44] P. E. Garrett, N. Warr, H. Baltzer, S. Boehmsdorff, D. G. Burke, M. Délèze, S. Drissi, J. Gröger, C. Günther, J. Kern, S. J. Mannanal, J. Manns, U. Müller, J.-P. Vorlet, and T. Weber, Nucl. Phys. **A611**, 68 (1996).